PAPER

Investigation of compressive strength of 3D-printed PLA/continuous glass fibers composites manufactured by simultaneous impregnation extrusion-based additive manufacturing

To cite this article: Amin Safi Jahanshahi *et al* 2025 *Eng. Res. Express* **7** 015403

Engineering Research Express

PAPER

Investigation of compressive strength of 3D-printed PLA/continuous glass fibers composites manufactured by simultaneous impregnation extrusion-based additive manufacturing

RECEIVED
13 October 2024

REVISED
8 December 2024

ACCEPTED FOR PUBLICATION
20 December 2024

PUBLISHED
6 January 2025

Amin Safi Jahanshahi[1], **Behnam Akhoundi**[1] and **Luca Quagliato**[2]

[1] Faculty of Mechanical Engineering, Sirjan University of Technology, Sirjan, Kerman, Iran
[2] Department of Mechanical and Biomedical Engineering, Ewha Womans University, Seoul, 03760, Republic of Korea

E-mail: Jahanshahi@sirjantech.ac.ir

Keywords: additive manufacturing, compressive strength, polylactic acid, continuous glass fibers, extrusion-based 3D printing

Abstract

The enhancement of stiffness and strength in additively manufactured components has garnered significant attention from scientists and engineers in recent years. This study explores the improvement of compressive strength in polylactic acid (PLA) composites reinforced with continuous glass fibers (CGFs) using a simultaneous impregnation extrusion-based additive manufacturing process. In this method, continuous fibers are introduced into the molten polymer through a side nozzle, coated with the polymer, and subsequently deposited onto the substrate or previously deposited layers. The primary advantage of this technique lies in its elimination of the need for pre-impregnated fibers, enabling the use of various continuous fiber types as reinforcing phases and different thermoplastics as matrices. To evaluate the impact of fiber orientation, fibers were aligned both parallel and perpendicular to the load direction, allowing an analysis of tensile lateral strain during compression. Compression test results revealed that neat PLA exhibited compressive strengths of 84.6 MPa and 72.3 MPa for parallel and perpendicular raster orientations, respectively. For the composite specimens, parallel fiber alignment resulted in delamination between the PLA matrix and fibers, with a compressive strength of 40.7 ± 1.2 MPa. Conversely, perpendicular fiber alignment increased compressive strength to 93 ± 1.1 MPa. The main innovation of this research is enhancing the compressive strength of composite samples by positioning continuous fibers perpendicular to the load direction within the samples. This arrangement induces transverse strain when the compressive force is applied, resulting in tensile stress being exerted on the continuous fibers, which in turn contributes to an increase in the compressive strength of the composite samples. Failure in these specimens occurred in regions where tensile strain direction changed, particularly at the corners of rounded-square cross-sections. This study demonstrates that aligning CGFs perpendicular to the loading direction enhances compressive strength by approximately 10.5%, introducing a bilinear elastic behavior and a more brittle-like fracture. The findings provide valuable insights for improving the crashworthiness and energy-absorbing capabilities of components in the automotive industry.

1. Introduction

Additive manufacturing (AM) is revolutionizing the way we design and produce objects. As AM technologies increasingly permeate everyday life, new opportunities and challenges continue to emerge [1–3]. This innovative technology enables the creation of complex shapes that were once unattainable with traditional manufacturing methods, promising to reshape the future of production [4, 5]. Key advantages of AM include:

- Customization: Facilitating intricate, one-of-a-kind designs tailored to specific needs.

- Flexibility: Allowing rapid adaptation of designs without costly retooling.
- Simplification: Streamlining product development by reducing design complexity.
- Efficient Spare Parts Management: Enabling on-demand production of replacements, reducing downtime and inventory costs.
- Faster Production: Accelerating lead times and product development cycles.
- Sustainability: Minimizing waste and promoting the use of eco-friendly materials [6–8].

Among AM techniques, Fused Filament Fabrication (FFF) stands out for its accessibility and ability to produce lattice structures, which are prized for their strength-to-weight ratio and suitability for lightweight applications [9]. FFF involves melting thermoplastic filament and depositing it layer by layer to build objects [10]. This method is particularly well-suited for crafting cellular structures and is recognized as environmentally friendly [11]. Recently, there has been growing interest in employing FFF for lattice structures due to its cost-effectiveness compared to techniques like Selective Laser Melting (SLM) and Electron Beam Melting (EBM) [10, 12, 13]. However, the success of FFF heavily depends on controlling process parameters, such as infill density, layer thickness, printing angles, and nozzle temperature, as these factors significantly influence the mechanical and physical properties of the final product [1, 13]. While PLA and ABS are commonly used materials in FFF, the technique is compatible with diverse thermoplastics like TPU, nylon, and HIPS, enabling broader design possibilities [14, 15]. Optimizing process parameters is critical to achieving desired strength and precision. Researchers have demonstrated that refining these parameters can enhance tensile and compressive strength, dimensional accuracy, and surface finish [16, 17]. For example, Sood *et al* [16] used a genetic algorithm to optimize ABS compressive strength, achieving 17.5 MPa. Similarly, Nancharaiah *et al* [18] employed the Taguchi method and ANOVA analysis to reveal that layer thickness and road width significantly influence the surface quality and dimensional accuracy of ABS parts. In addition, alternative materials like PETG and PEEK have shown promise. Zaman *et al* [19] demonstrated PETG's superior compressive strength compared to ABS, while Wu *et al* [17] highlighted PEEK's improved mechanical properties over ABS in FFF applications.

A growing body of research emphasizes optimizing process parameters and exploring new materials to unlock FFF's potential. For example, Tang *et al* [20], Rosli *et al* [21], and Dong *et al* [22] investigated the effects of nozzle temperature, layer thickness, and printing speed on the mechanical properties of PLA and ABS lattice structures. These studies revealed optimization opportunities but also underscored the need for further exploration of additional parameters. Aloyaydi *et al* [23] examined infill patterns and build orientations, finding that grid patterns provided the highest compressive strength, while triangular patterns exhibited the greatest stiffness.

Research has also focused on reinforcement methods. Pazhamannil *et al* [24] and Mohammadizadeh *et al* [25] explored the effects of material selection and reinforcement on mechanical performance. For instance, short carbon fiber-reinforced nylon composites were shown to outperform pure nylon in tensile and flexural properties but had lower compressive strength. Variations in mechanical behavior are common in thermoplastics [26] and more complex multi-material structures [27] though these effects remain insufficiently studied for FFF processes [28] In rare studies such as that by Araya-Calvo *et al* [29], carbon fiber-reinforced polyamide-6 matrices using isotropic and concentric patterns demonstrated significant stiffness improvements but also increased embrittlement. The reinforcement patterns, distribution, and orientation significantly influenced compressive and flexural properties, emphasizing the importance of minimizing layer delamination to enhance performance. Further contributions in this field continue to advance our understanding of material properties in additively manufactured components. Sears *et al* [30] studied scaffolds made of propylene fumarate dimethacrylate polyHIPEs with shells composed of PLA and polycaprolactone (PCL), evaluating their compressive mechanical properties. The results indicated that scaffolds with PCL shells exhibited a compressive modulus of 30 MPa and a compressive strength of 3 MPa, whereas scaffolds with PLA shells demonstrated higher values of 100 MPa and 10 MPa, respectively. Francis and Jain [31] investigated the compressive mechanical properties of clay-based polymer nanocomposites, focusing on the impact of double extrusion on the material's performance. By employing a double extrusion system, the mixing of nanoclay was improved, leading to increases of 14.5% in tensile strength, 21% in tensile modulus, and 24% in compressive strength of the printed samples.

Petousis *et al* [32] explored the effect of compressive loading rates on the mechanical behavior of four widely used thermoplastic polymers in extrusion-based 3D printing: polycarbonate (PC), polyethylene terephthalate glycol (PETG), polymethyl methacrylate (PMMA), and thermoplastic polyurethane (TPU). Compressive tests conducted at strain rates ranging from 1.3 to 200 mm min^{-1} revealed that increasing the strain rate led to a 40% increase in the compressive strength of PMMA and a 29% increase in the compressive modulus of TPU. Among the materials tested, PC exhibited the highest sensitivity to strain rates. Gui *et al* [33] optimized the compressive mechanical properties of polyimide aerogels by employing a 3D printing method based on extrusion with freeze casting. The maximum

compressive strength and modulus of the printed polyimide aerogel samples were enhanced to 6.35 MPa and 63.5 MPa, respectively. Vijayasankar *et al* [34] evaluated the mechanical properties of PETG composites reinforced with silk fibers at weight percentages of 2%, 5%, and 10%. They reported that while printing with 10% silk fibers presented challenges, the compressive modulus of the composite with 2% silk fibers increased by 60% compared to neat PETG. Zarei *et al* [35] examined the mechanical properties of PLA-Ti6Al4V (Ti64) composites. Their findings indicated that adding Ti64 increased the glass transition temperature of PLA but slightly reduced the melting temperature, crystallization temperature, and thermal stability of the rasters. Notably, the addition of 3% to 6% by weight of Ti64 increased the compressive strength and modulus of the composite to 49.9 MPa and 1.9 GPa, respectively. Lastly, Mohamed *et al* [36] studied the influence of printing parameters on the creep displacement of PC-ABS blends. The results showed that minimum creep displacement was achieved under specific conditions: a layer height of 0.2540 mm, a raster angle of 0°, a print direction of 20°, eight shells, and an extrusion width of 0.4572 mm.

Kong *et al* [37] evaluated the mechanical properties of bi-matrix composites with a multi-cavity structure reinforced with continuous fibers produced by a 3D printer. They used continuous carbon fibers and Basalt, continuous carbon fibers pre-impregnated with epoxy resin, and PLA and PA filaments to print the samples. They stated that after printing, continuous carbon fibers pre-impregnated with epoxy resin have the most effect on mechanical properties and failure mode. The main failure mode in this research was reported as pullout and fiber breakage. Khan *et al* [38] investigated the fracture toughness of 3D-printed polymer matrix composites reinforced with different fibers. They considered two materials PLA and PEEK as matrices with low and high melting temperatures. They stated that parameters such as printing temperature, fiber volume percentage, length of fibers, square shape of the nozzle, annealing, suitable surface treatment on fibers, printing in several directions, and printing in a vacuum have positive effects and parameters such as printing speed, layer thickness, cavities and the porosity, and circular shape of the nozzle have negative effects on the mechanical properties and fracture performance of the printed samples. By presenting a 3D G-code, Akhoundi *et al* [1] succeeded in the deposition of continuous glass fibers on curved surfaces with the simultaneous fiber-polymer impregnation method. Ulkir [39] investigated the mechanical and thermal properties of 3D printed composites reinforced with copper, bronze, and microcarbon fibers. The results showed that the highest tensile strength was obtained at a layer thickness of 0.1 mm, a filling percentage of 60%, and a nozzle temperature of 230 °C. Also, the metal reinforcing particles reduced the strength and increased the elongation. In addition, the highest heat resistance is related to PLA-Cu composite material. Saravanamuthkumar *et al* [40] investigated the effect of printing parameters on the compressive properties of multi-material composites including PLA and PLA reinforced with almond shell. The maximum compressive strength obtained was 35.41 MPa at a printing speed of 20 mm s^{-1}, a layer height of 0.1 mm, and a printing temperature of 200 °C. Liu *et al* [41] investigated the properties of PEEK-glass continuous fiber composites made by the AM method. The maximum tensile strength, bending strength, interlaminar shear strength, and impact strength were 703 MPa, 562 MPa, 44 MPa, and 180 Kj/m^2, respectively. Ulkir *et al* [42] investigated the effect of printing temperature on the mechanical properties of 3D-printed ABS. They stated that as the temperature increases from 220 to 270 °C (increase by 10 °C), the mass of the printed samples as well as the tensile strength decreases almost linearly. The maximum tensile strength at a printing temperature of 220 °C is equal to 24.6 MPa and the minimum tensile strength at a printing temperature of 270 °C is 14.4 MPa. Alomarah *et al* [43] investigated the effect of FFF and multi-jet fabrication techniques on the mechanical properties of auxetic structures and the ability of printed parts to absorb energy.

Based on a thorough review of the existing literature, the primary focus of this contribution is the investigation of the viability of employing continuous glass fibers (CGF)s as reinforcement of a Polylactic Acid (PLA) [44] and subsequently investigating elastic, failure, and fracture properties of the resulting composite. This study is the first to investigate the fracture behavior of 3D-printed PLA composites reinforced with continuous glass fibers. The main question of this research is expressed as whether continuous fibers in a 3D printed composite material can cause a change in compressive mechanical properties and how this increase or decrease in compressive mechanical properties is related to continuous fibers. Parallel and perpendicular configurations have been tested to account for the deposition strategy effect on the compression load direction. In addition, the fracture surfaces of unfilled and reinforced PLA have been analyzed by Scanning Electron Microscope (SEM) and show that by changing the direction of the fibers, the compressive load distribution can be changed to the tensile deformation, and the mechanical compressive properties of the composite sample can be improved, resulting in an improvement of the compressive strength of ~10% and a change in the overall material behavior.

2. Materials and methods

This study utilizes polylactic acid (PLA) filament (Sizan, Iran) as the matrix material. According to the producer's datasheet, the glass transition temperature of the filament is 80°C. E-glass continuous fiber yarn (CGF: Jiahe Taizhou Co., China) was used as the reinforcement, with a mass per length of 0.1 g m^{-1} and a bundle

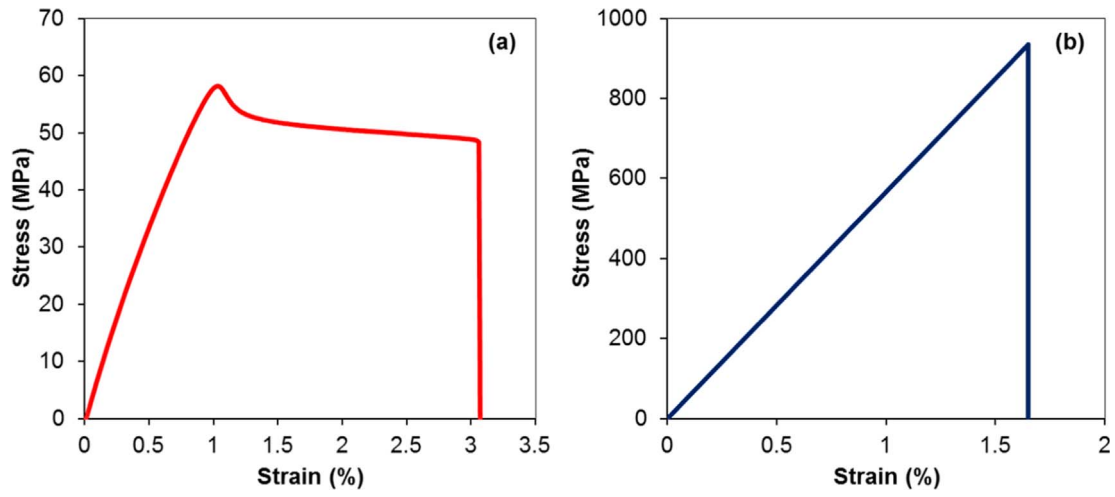

Figure 1. Tensile stress–strain curve for (a) PLA and (b) continuous E-glass fibers [45].

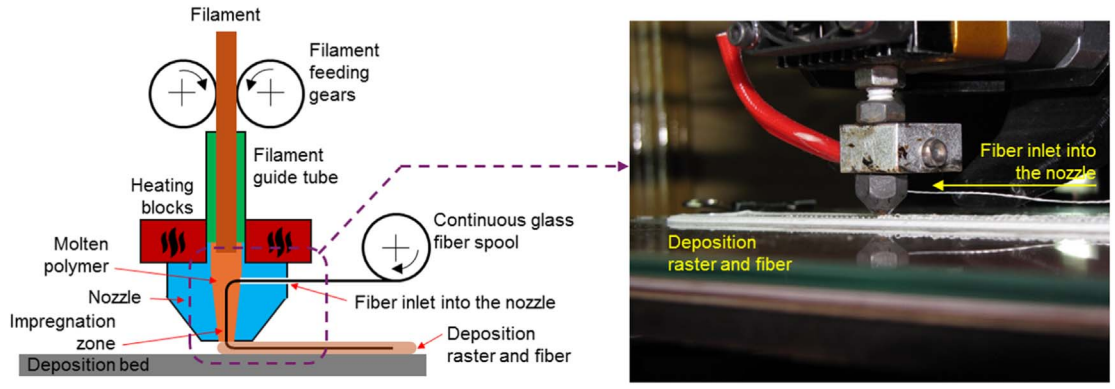

Figure 2. Schematics of the simultaneous impregnation extrusion process and detail of the implemented FFF process where the CGF is fed to the nozzle during the extrusion.

diameter of 0.22 mm (Tex 800, fiber diameter of 8 microns). The datasheet specifies a density of 2.5 g cm^{-3}, a nominal tensile strength of 1000 MPa, and a tensile modulus of 60 GPa for the E-glass fiber yarn.

To verify these mechanical properties, tensile tests were conducted according to ASTM D2256, confirming a tensile strength of 935 MPa, a tensile modulus of 56.7 GPa, and a tensile fracture strain of 0.0165 [45]. The Tensile stress–strain curve for PLA (averaged from 5 samples) and continuous glass fibers (averaged from 10 samples) obtained from tensile tests is shown in figure 1.

In the employed simultaneous impregnation extrusion (SIE) process, continuous glass fibers are fed into the 3D printer nozzle, where they are impregnated with the molten PLA polymer and deposited onto the substrate, as illustrated in figure 2. Manufacturing was performed using a Quantum 2020 3D printer (Iran) with a bed size of 200 × 200 × 200 mm, targeting a fiber volume percentage of 30%. To experimentally determine the fiber volume percentage, samples were burned after mechanical testing, and the remaining glass fibers were weighed after washing and drying. The weight percentage of fibers was then converted to volume percentage following ASTM D3171. For the PLA/CGF composite samples, the experimentally calculated fiber volume percentage was 30.5%, indicating a minor deviation of approximately 2% from the theoretical target.

Since the presence of fibers reduces the available extruded polymer volume, the PLA filament feeding speed had to be adjusted to maintain uniform printing and prevent overflow. After calibration, the optimal printing speed for the PLA-CGF composite was determined to be 10 mm s^{-1}, ensuring consistent deposition without material shortages or excesses. To evaluate mechanical properties, five samples were printed for each test, and the average results were reported.

As the nozzle temperature increases, the viscosity of the polymer material decreases, enhancing the impregnation of continuous fibers and polymer materials. However, excessive nozzle temperatures can lead to polymer degradation, negatively impacting the surface quality along the build direction. Based on prior studies using the same material [45]. A

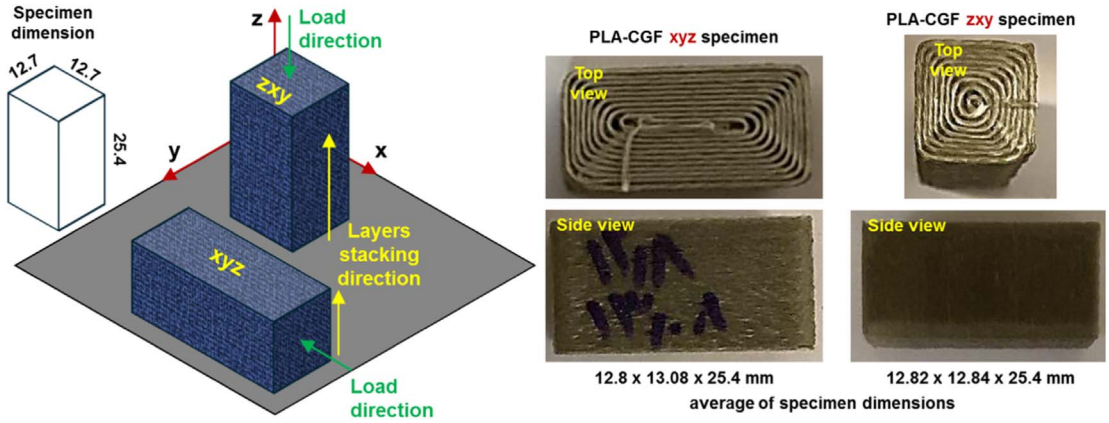

Figure 3. Stacking directions for the PLA-CGF specimens considering the 'XYZ' and 'ZXY' orientations and printed specimens where fibers and raster denote the layer's stacking direction.

Table 1. Process parameters for the composite (PLA-CGF) and unfilled PLA 3D printing.

Parameter	Value
Nozzle temperature [°C]	220
Deposition bed temperature [°C]	60
Nozzle diameter [mm]	0.5
Extrusion width (raster) [mm]	0.58
Extrusion layer height (raster) [mm]	0.22
Filament feeding speed [mm/s]	40/10
Neat polymer/PLA-CGF composite	
Extrusion multiplier	0.7

nozzle temperature of 220 °C was employed in this research to strike a balance between fiber impregnation and material integrity. The substrate temperature also plays a crucial role in ensuring proper inter-raster and inter-layer bonding, particularly for the primary layers. It is essential to keep the substrate temperature below the glass transition temperature of the polymer (80 °C for the PLA material used in this study) to prevent substrate softening and unintentional detachment from the bed. Considering this, the bed temperature was set to 60 °C [46]. Additionally, the height of the layers must be carefully chosen relative to the diameter of the fibers. If the layer height is less than the fiber diameter, the fibers are likely to be damaged during manufacturing. Conversely, an excessively high nozzle height can create voids within the printed sample, increasing surface roughness in the build direction [45]. To mitigate these issues, the layer height in this research was set equal to the fiber diameter, 0.22 mm, and the extrusion width was set to 0.58 mm, corresponding to a fiber volume percentage of 30%. The fiber volume percentage relative to the matrix volume was calculated using equation (1) [45] where V_f is the fiber volume percentage, d_f is the diameter of the fibers, w is the extrusion width and h is the layer height.

$$V_f = (\pi d_f^2/4 \cdot w \cdot h) \times 100 \tag{1}$$

Moreover, since the fibers are extruded alongside the polymer matrix, it is essential to reduce the amount of polymer to maintain consistent extrusion. In such cases, the filament feed parameter, denoted by the letter 'E' in the G-code, must be adjusted by multiplying it with a coefficient known as the extrusion multiplier. The value of the extrusion multiplier (F) is calculated using equation (2) [1, 45].

$$F = 1 - V_f \tag{2}$$

The overall manufacturing settings are summarized in table 1, covering both the composite material and the unfilled PLA used as a benchmark to compare the compressive properties of the composite. To evaluate the compressive properties, specimens were manufactured following ASTM D695 specifications, with a square cross-section measuring 12.7 mm and a height of 25.4 mm, as shown in figure 3.

To assess the effectiveness of the CGF reinforcement, two sets of specimens were produced. The first set, referred to as 'XYZ', features a growing trajectory throughout the specimen height. This configuration causes part of the fibers to experience tensile strains and another part to experience compressive strains during load application along the x-direction (the load direction).

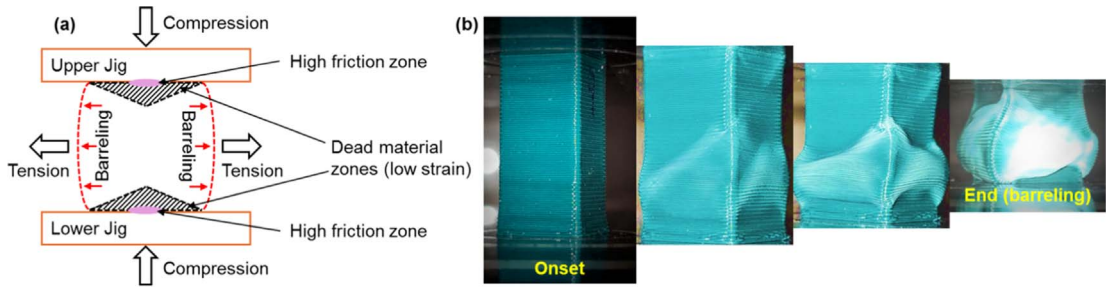

Figure 4. (a) Schematic explanation of the deformation behavior in uniaxial compression test and (b) barreling occurrence on neat PLA specimens at the end of the compressive test.

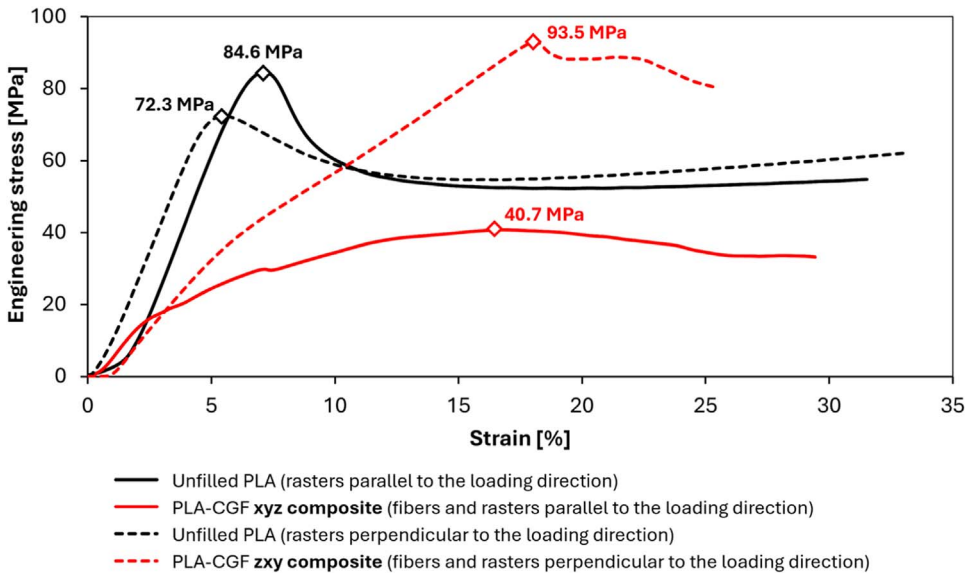

Figure 5. Engineering stress versus percentage elongation of the compression tests on unfilled PLA and composite PLA-CGF compression specimens. Peak strengths are highlighted in the chart.

The second set of specimens, referred to as 'ZXY', featured fibers aligned in a concentric pattern, plane by plane, oriented perpendicularly to the z-direction (load direction) during compression tests. As previously described, unfilled PLA specimens with the same raster alignment as the composite PLA-CGF specimens were also manufactured and used as benchmarks. Compression tests for both unfilled PLA and composite PLA-CGF specimens were conducted using a SANTAM 20 machine (Iran) at a compression speed of 5 mm/min. Following the tests, the failure surfaces were analyzed using a Prox-Phenom G6 Scanning Electron Microscope (SEM) to examine the roles of the fibers, the matrix, and their interaction during load application.

3. Results and discussion

This section begins by presenting the results of the compression tests conducted on both unfilled PLA and composite PLA-CGF materials. This is followed by an analysis of the failure surfaces using SEM, along with relevant observations and interpretations of the results. Finally, the energy absorption characteristics of the printed samples are discussed.

3.1. Compressive test results

In the uniaxial compression test, a force is applied vertically on the top of the specimen resulting in the rise of both compressive and tensile deformations. In addition, due to the friction interaction between the upper and lower jigs and the specimen, an almost negligible deformation zone, known as the dead material zone, appears in the vicinity of the contact area, whereas barreling occurs on the sides of the specimen, figure 4.

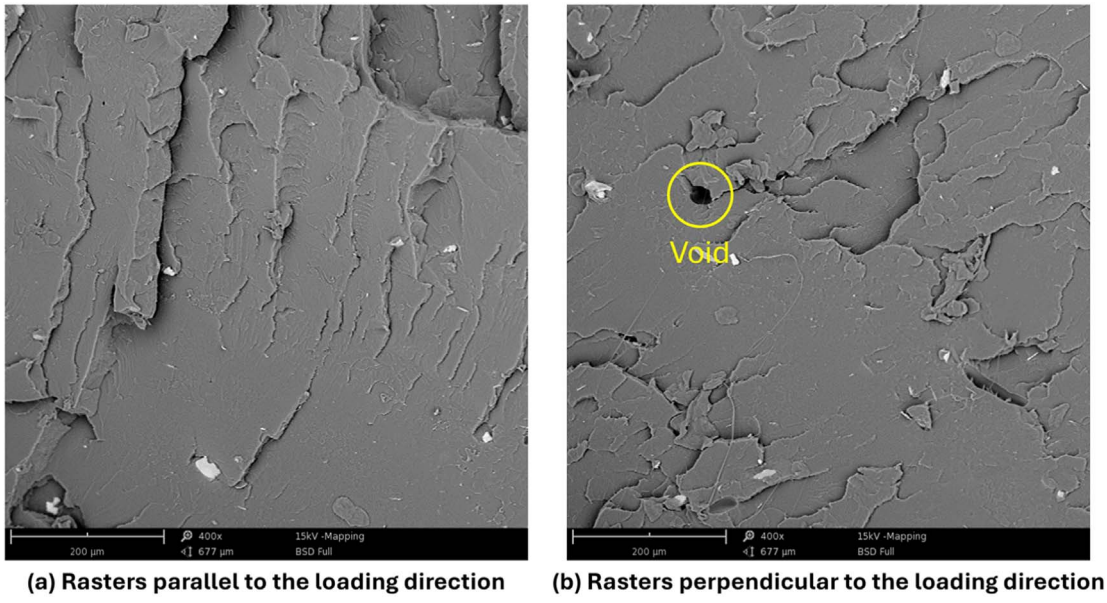

Figure 6. SEM images of cross-sectional of neat polymer (a) Unfilled PLA (rasters parallel to the loading direction), (b) Unfilled PLA (rasters perpendicular to the loading direction).

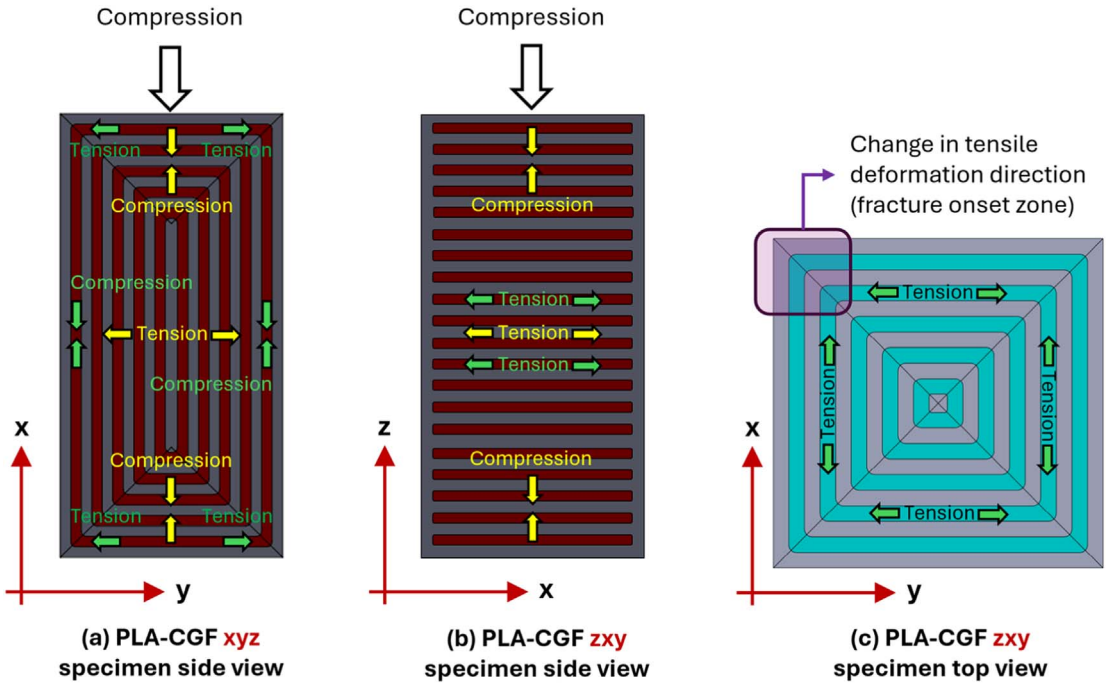

Figure 7. Tensile and compressive behavior for the PLA-CGF composite for the (a) XYZ specimen (front view), (b) ZXY specimen (front view), and ZXY specimen (top view).

Consequently, both compressive and tensile deformations coexist within the specimen during the test. Additionally, the deformation behavior changes significantly in composite materials, such as PLA-CGF, due to the differing responses of the individual components in the composite and their interactions. Focusing on the results of the compression tests for both unfilled PLA and PLA-CGF composite specimens, the average stress–strain curves from five test repetitions are presented in figure 5.

For unfilled PLA specimens, the alignment of the rasters with the compressive load direction results in an approximately 17% increase in strength. This improvement is attributed to the partial orientation of the rasters, which act as independent load-bearing units during compression. Conversely, when the rasters are deposited plane by plane perpendicular to the compression direction, their behavior is considered isotropic. Regardless of the raster alignment, neat PLA specimens fail under buckling conditions. SEM images of the cross-sections of

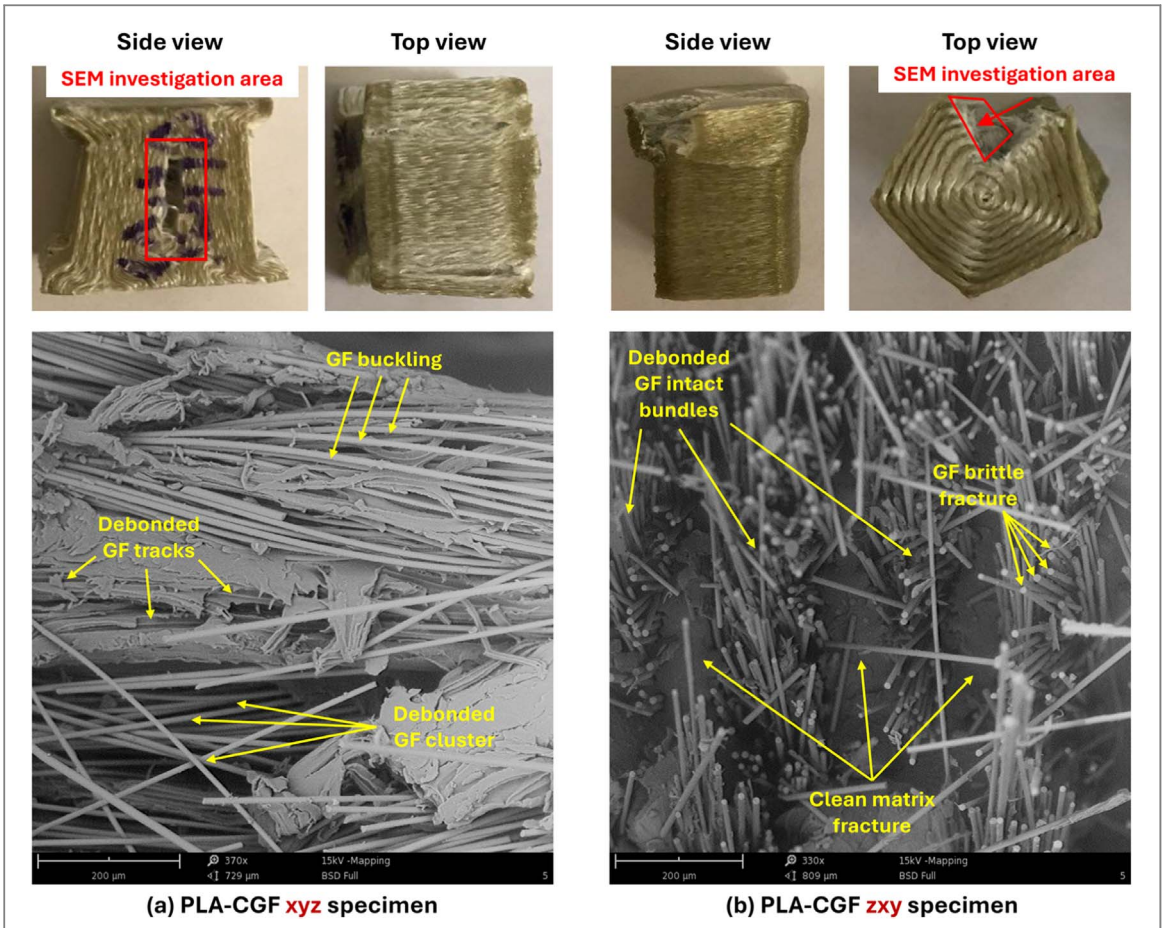

Figure 8. Compression specimens after compressive failure (side and top views) and SEM image analysis for PLA-CGF specimens manufactured by (a) XYZ and (b) ZXY fibers alignments.

neat PLA samples are shown in figure 6. Since these samples did not fail during the compression tests, they were frozen in liquid nitrogen and subsequently fractured for analysis. The cross-sectional images confirm that the chosen printing parameters were appropriate, as no significant voids were observed in the connections between rasters or layers. The compressive strengths and moduli for the two unfilled PLA specimens are:

- Parallel rasters: 84.6 ± 1.1 MPa and 1.8 ± 0.04 GPa.
- Perpendicular rasters: 72.3 ± 0.9 MPa and 1.7 ± 0.05 GPa.

For PLA-CGF compression specimens, the variation in stress versus percentage strain and compressive strength is strongly influenced by the deposition strategy and its interaction with the applied compressive load. In the case of the XYZ specimens (figure 3), the dead material zone experiences tensile deformation in the continuous fibers and compressive deformation in the polymer matrix. In contrast, in the rest of the specimen, particularly near its center where barreling occurs, both fibers and matrix are under compression along the *x*-axis, while the matrix experiences tension in the y and z directions (figure 7(a)). As a result, failure in the XYZ PLA-CGF specimens is expected to occur in the central region, away from the dead material zone. This failure results from tensile deformation in the PLA matrix and concurrent compressive deformation in the fibers, leading to buckling and debonding at the fiber-matrix interface. For this configuration, the compressive strength improvements over unfilled PLA are quantified as 10.5% and 29.3%, depending on the raster orientation relative to the applied compressive load. Additionally, the stress–strain relationship exhibits a shift from the single-peak stress followed by softening, typical of unfilled PLA specimens, to a bilinear behavior. This bilinear response is characteristic of multi-material structures, where distinct differences in the elastic and elastic-plastic behavior between the neat matrix and composite samples are evident [27].

In contrast, for the ZXY specimens, the rasters and continuous glass fibers are oriented perpendicularly to the compressive load. This orientation results in lower reinforcement effectiveness compared to the XYZ configuration. As shown in figure 5, the presence of CGFs smooths the stress–strain relationship, producing a

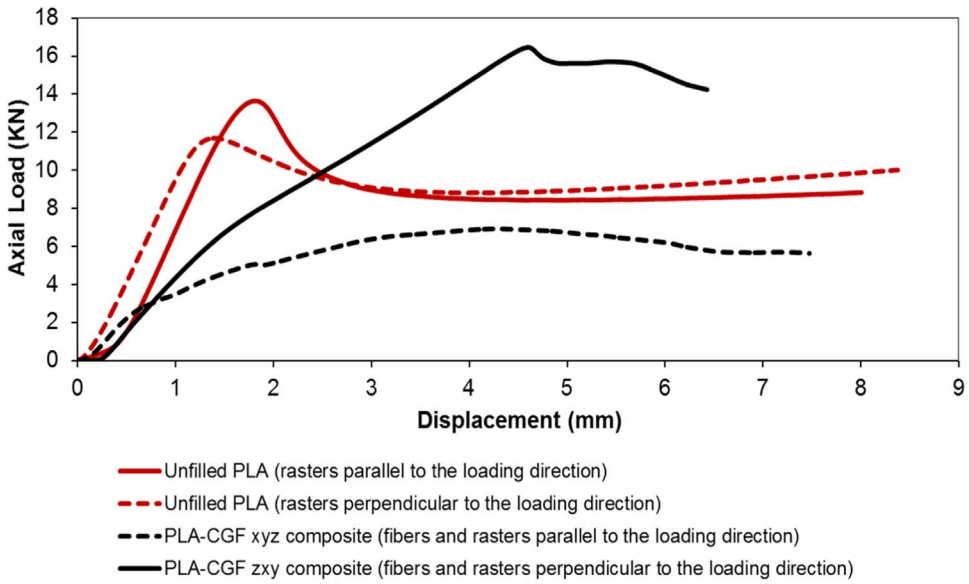

Figure 9. Axial force versus Displacement of the compression tests on unfilled PLA and composite PLA-CGF compression specimens.

monotonic increase in stress until reaching the maximum value, followed by slight softening prior to failure. In this configuration, compression occurs along the *z*-axis, while tension exists in the fibers and matrix along the x and y directions (figure 7(b)). With the fibers lying in the xy planes under tension, debonding is most likely to occur at the square corners where the tension direction transitions from x to y (figure 7(c)). Furthermore, since both fibers and rasters are oriented perpendicularly to the compressive load, the fibers do not act as reinforcements but rather as inclusions, leading to a matrix-dominated fracture in the PLA-CGF composite. The 2.3-fold difference in strength between the XYZ and ZXY configurations highlights the typical behavior of composite materials, emphasizing the effectiveness of CGFs in enhancing the properties of the PLA matrix. To summarize, the compressive strength and modulus are as follows:

- PLA-CGF (XYZ): 40.7 ± 1.2 MPa and 0.88 ± 0.02 GPa.
- PLA-CGF (ZXY): 93.5 ± 1.1 MPa and 0.86 ± 0.01 GPa.

SEM analyses were conducted to further investigate the behavior of the two tested configurations of PLA-CGF composites and to confirm the hypotheses regarding deformation, debonding, and buckling. The results are presented in figure 8. As shown in figure 8(a), the XYZ composite exhibits separation at the center of the specimen, where the PLA matrix is subjected to tensile stresses. This tensile stress causes debonding between the PLA matrix and the CGFs. Additionally, as hypothesized, the tensile deformation in the PLA matrix induces buckling of the glass fibers, which then debond from the matrix, leaving visible tracks throughout the fracture surface.

In contrast, the ZXY composite demonstrates the negligible role of the CGFs in bearing the compressive load during the test. As illustrated in figure 8(b), the fracture surface is characterized by clean matrix separation with minimal fibrillation [26]. Furthermore, a fiber pull-out phenomenon is observed, where fibers detach from the matrix in bundles, reflecting their deposition pattern during the FFF process.

3.2. Energy absorption properties

The force-displacement diagram of the samples is presented in figure 9, showing behavior similar to that observed in the stress–strain diagram. Based on the data from figure 9, the crushing properties of the samples—including initial peak force, mean crush force, total absorbed energy, specific absorbed energy, and crushing force efficiency—are summarized in table 2. The composite sample with fibers oriented perpendicularly to the load direction exhibits the highest initial peak force and mean crush force values. This can be attributed to the higher compressive strength of the sample, which is influenced by the transverse strain. Conversely, the total absorbed energy and specific absorbed energy are greater for the unfilled PLA samples compared to the composite samples. This suggests that while the composite samples demonstrate improved compressive strength, their energy absorption characteristics may require further optimization. To this end, it can be concluded that by optimizing the geometry of the composite samples, the influence of geometry on crushing parameters and overall crashworthiness can be better understood and improved.

Table 2. Crushing properties of the unfilled PLA and composite PLA-CGF compression specimens.

	Sample			
Crushing Properties	Unfilled PLA (rasters parallel to the loading direction)	Unfilled PLA (rasters perpendicular to the loading direction)	PLA-CGF xyz composite (fibers and rasters parallel to the loading direction)	PLA-CGF zxy composite (fibers and rasters perpendicular to the loading direction)
Initial Peak Force (KN)	13.65	11.69	6.91	16.46
Mean Crush Force (KN)	8.34	8.90	5.44	10.69
Total Absorb Energy (J)	66.78	74.58	40.71	68.74
Specific Absorbed Energy (J/g)	13.04	14.57	6.04	10.20
Crushing Force Efficiency	0.61	0.76	0.79	0.65

4. Conclusions

This study investigated the compressive mechanical properties and fracture behavior of CGF-reinforced PLA composites manufactured using a custom SIE process. The results demonstrated that orienting CGFs parallel to the load direction enhances the compressive strength of unfilled PLA by 10.5% to 29.3%. Conversely, when CGFs are oriented perpendicularly to the load direction, their reinforcing effect diminishes significantly, causing the matrix to lose both strength and toughness. The PLA-CGF composite exhibited distinct mechanical behavior compared to unfilled PLA, showing a bilinear quasi-brittle behavior in the parallel configuration and low hardening with low yield in the perpendicular configuration. These findings highlight the critical role of CGF orientation in determining the mechanical performance of the composite. Moreover, this research showcased the effectiveness of the SIE process for fabricating composite materials, even with sharp (90°) turns, and demonstrated the potential improvements achievable with CGFs. The experimental results emphasize that the direction of the continuous filler is pivotal to the mechanical characteristics of 3D-printed composite materials. For the PLA-CGF ZXY composite, the initial peak force and mean crush force were found to be 16.46 KN and 10.69 KN, respectively representing 30% and 24% increases, respectively, compared to unfilled PLA samples. These results indicate the potential of PLA-CGF composites for improving the crashworthiness of energy-absorbing components. Future research should focus on exploring the influence of the fiber volume percentage on compressive mechanical properties, as well as the use of high-modulus reinforcements, such as continuous carbon fibers. This line of investigation could further enhance the crashworthy performance of energy-absorbing components across various industries.

Conflicts of interest

The authors declare no conflicts of interest.

Data availability statement

The data cannot be made publicly available upon publication because no suitable repository exists for hosting data in this field of study. The data that support the findings of this study are available upon reasonable request from the authors.

ORCID iDs

Amin Safi Jahanshahi https://orcid.org/0009-0001-9417-5535
Behnam Akhoundi https://orcid.org/0000-0002-4283-1684
Luca Quagliato https://orcid.org/0000-0002-5379-8306

References

[1] Akhoundi B, Jahanshahi A S and Abbassloo A 2024 G-code generation for deposition of continuous glass fibers on curved surfaces using material extrusion-based 3D printing *Eng. Res. Express* **6** 015401
[2] Perin M, Quagliato L, Berti G A, Jang C, Jang S and Lee T 2023 Manufacturing process, tensile-compressive, and impact properties of tungsten (W)-particle-reinforced SLA methacrylate *Polymers* **15** 4728
[3] Samykano M, Kumaresan R, Kananathan J, Kadirgama K and Pandey A K 2024 An overview of fused filament fabrication technology and the advancement in PLA-biocomposites *Int. J. Adv. Manuf. Technol.* **132** 27–62
[4] Mehrpouya M, Dehghanghadikolaei A, Fotovvati B, Vosooghnia A, Emamian S S and Gisario A 2019 The potential of additive manufacturing in the smart factory industrial 4.0: a review *Applied Sciences* **9** 3865
[5] Sathies T, Senthil P and Anoop M 2020 A review on advancements in applications of fused deposition modelling process *Rapid Prototyping Journal* **26** 669–87
[6] Ford S and Despeisse M 2016 Additive manufacturing and sustainability: an exploratory study of the advantages and challenges *J. Clean. Prod.* **137** 1573–87
[7] Liu P, Huang S H, Mokasdar A, Zhou H and Hou L 2014 The impact of additive manufacturing in the aircraft spare parts supply chain: supply chain operation reference (scor) model based analysis *Production Planning & Control* **25** 1169–81
[8] Singh D, Singh R and Boparai K 2022 Investigations for surface roughness and dimensional accuracy of biomedical implants prepared by combining fused deposition modelling, vapour smoothing and investment casting *Advances in Materials and Processing Technologies* **8** 843–62
[9] Akhoundi B and Modanloo V 2023 Investigation and feasibility of printing polyoxymethylene semi-crystalline polymer parts with fused filament fabrication 3D printer and evaluation of mechanical properties of the printed samples *J. Mater. Eng. Perform.* **33** 9396–405
[10] Costa S F, Duarte F M and Covas J A 2017 Estimation of filament temperature and adhesion development in fused deposition techniques *J. Mater. Process. Technol.* **245** 167–79
[11] Cuan-Urquizo E and Guerra Silva R 2023 Fused filament fabrication of cellular, lattice and porous mechanical metamaterials: a review *Virtual and Physical Prototyping* **18** e2224300

[12] Feng Q *et al* 2018 Quasi-static analysis of mechanical properties of Ti6Al4V lattice structures manufactured using selective laser melting *Int. J. Adv. Manuf. Technol.* **94** 2301–13
[13] Samykano M, Selvamani S K, Kadirgama K, Ngui W K, Kanagaraj G and Sudhakar K 2019 Mechanical property of FDM printed ABS: influence of printing parameters *Int. J. Adv. Manuf. Technol.* **102** 2779–96
[14] Chadha A, Ul Haq M I, Raina A, Singh R R, Penumarti N B and Bishnoi M S 2019 Effect of fused deposition modelling process parameters on mechanical properties of 3D printed parts *World Journal of Engineering* **16** 550–9
[15] Dey A and Yodo N 2019 A systematic survey of FDM process parameter optimization and their influence on part characteristics *Journal of Manufacturing and Materials Processing* **3** 64
[16] Sood A K, Ohdar R K and Mahapatra S S 2012 Experimental investigation and empirical modelling of FDM process for compressive strength improvement *J. Adv. Res.* **3** 81–90
[17] Wu W, Geng P, Li G, Zhao D, Zhang H and Zhao J 2015 Influence of layer thickness and raster angle on the mechanical properties of 3D-printed PEEK and a comparative mechanical study between PEEK and ABS *Materials* **8** 5834–46
[18] Nancharaiah T, Raju D R and Raju V R 2010 An experimental investigation on surface quality and dimensional accuracy of FDM components *Int. J. Emerg. Technol.* **1** 106–11 (https://researchtrend.net/ijet/ijet12/20.pdf)
[19] Zaman U K, Boesch E, Siadat A, Rivette M and Baqai A A 2019 Impact of fused deposition modeling (FDM) process parameters on strength of built parts using Taguchi's design of experiments *Int. J. Adv. Manuf. Technol.* **10** 1215–26
[20] Tang C, Liu J, Yang Y, Liu Y, Jiang S and Hao W 2020 Effect of process parameters on mechanical properties of 3D printed PLA lattice structures *Composites* C **3** 100076
[21] Rosli N A, Hasan R, Alkahari M R and Tokoroyama T 2017 Effect of process parameters on the geometrical quality of ABS polymer lattice structure *Proc. SAKURA Symp. Mech. Sci. Eng.* 3–5
[22] Dong G, Wijaya G, Tang Y and Zhao Y F 2018 Optimizing process parameters of fused deposition modeling by Taguchi method for the fabrication of lattice structures *Additive Manufacturing* **19** 62–72
[23] Aloyaydi B, Sivasankaran S and Mustafa A 2020 Investigation of infill-patterns on mechanical response of 3D printed poly-lactic-acid *Polym. Test.* **87** 106557
[24] Pazhamannil R V, Krishnan C N and Edacherian P G 2022 A. Investigations into the effect of thermal annealing on fused filament fabrication process *Advances in Materials and Processing Technologies* **8** 710–23
[25] Mohammadizadeh M, Gupta A and Fidan I 2021 Mechanical benchmarking of additively manufactured continuous and short carbon fiber reinforced nylon *J. Compos. Mater.* **55** 3629–38
[26] Quagliato L, Ricotta M, Zappalorto M, Ryu S C and Kim N 2022 Notch effect in 20% short carbon fibre-PA reinforced composites under quasi-static tensile loads *Theor. Appl. Fract. Mech.* **122** 103649
[27] Jang S, Quagliato L and Kim N 2022 Experimental and numerical investigations on the failure behavior of metal skin and carbon fiber-reinforced polymer core structures considering layup and manufacturing process conditions *Adv. Compos. Mater* **31** 173–94
[28] Chicos L-A *et al* 2022 Fused filament fabrication of short glass fiber-reinforced polylactic acid composites: infill density influence on mechanical and thermal properties *Polymers* **14** 4988
[29] Araya-Calvo M *et al* 2018 Evaluation of compressive and flexural properties of continuous fiber fabrication additive manufacturing technology *Additive Manufacturing* **22** 157–64
[30] Sears N, Dhavalikar P, Whitely M and Cosgriff-Hernandez E 2017 Fabrication of biomimetic bone grafts with multi-material 3D printing *Biofabrication* **9** 025020
[31] Francis V and Jain P K 2018 On the improved mechanical properties of nanoclay reinforced ABS composite for fused deposition modelling *Int. J. Mater. Prod. Technol.* **57** 20–42
[32] Petousis M *et al* 2023 A coherent assessment of the compressive strain rate response of PC, PETG, PMMA, and TPU thermoplastics in MEX additive manufacturing *Polymers* (https://doi.org/10.3390/polym15193926)
[33] Gui Y *et al* 2023 High-strength and multifunctional honeycomb polyimide aerogel fabricated by a freeze casting-assisted extrusion printing and building block-assembly strategy for sound absorbing metamaterials *Additive Manufacturing* **77** 103799
[34] K N V, Bonthu D, Doddamani M and Pati F 2022 Additive manufacturing of short silk fiber reinforced PETG composites *Materials Today Communications* **33** 104772
[35] Zarei M *et al* 2023 Enhanced bone tissue regeneration using a 3D-printed poly(lactic acid)/Ti6Al4V composite scaffold with plasma treatment modification *Sci. Rep.* **13** 3139
[36] Mohamed O A, Masood S H and Bhowmik J L 2017 Experimental investigation of time-dependent mechanical properties of PC-ABS prototypes processed by FDM additive manufacturing process *Mater. Lett.* **193** 58–62
[37] Kong H *et al* 2023 An investigation into mechanical properties of a 3D printed two-matrix continuous fiber composites with multi-cavity structure *Journal of Materials Research and Technology* **26** 4365–86
[38] Khan T *et al* 2024 Recent developments in improving the fracture toughness of 3D-printed fiber-reinforced polymer composites *Composites* B **283** 111622
[39] Ulkir O 2024 Investigation on the mechanical and thermal properties of metal-PLA composites fabricated by FDM *Rapid Prototyping Journal* **30** 2113–22
[40] Saravanamuthukumar P *et al* 2024 Compressive strength performance of 3D printed PLA/almond shell particles reinforced PLA multi-material composite *J. Elastomers Plast.* **56** 786–806
[41] Liu X *et al* 2024 Mechanical and dielectric properties of continuous glass fiber reinforced poly-ether-ether-ketone composite components prepared by additive manufacturing *Additive Manufacturing* **81** 103978
[42] Ulkir O, Ertugrul I, Ersoy S and Yağımlı B 2024 The effects of printing temperature on the mechanical properties of 3D-printed acrylonitrile butadiene styrene *Appl. Sci.* **8** 543
[43] Alomarah A, Abbas A T, Faisal B, Peng Z and Ruan D 2024 The effects of manufacturing techniques on the mechanical performance of an auxetic structure manufactured by fused filament fabrication and multijet fusion processes *Adv. Eng. Mater.* **26** 2302033
[44] Wang Y, Lyu C, Zhang Q, Li W and Liu J 2021 Preparation and performance index test of continuous glass fiber reinforced filament-polylactic acid for 3D printer *Journal of Physics: Conf. Series* (IOP Publishing) 012053
[45] Akhoundi B, Behravesh A H and Bagheri Saed A 2020 An innovative design approach in three-dimensional printing of continuous fiber–reinforced thermoplastic composites via fused deposition modeling process: in-melt simultaneous impregnation *Proc. Inst. Mech. Eng.* B **234** 243–59
[46] Akhoundi B, Behravesh A H and Bagheri Saed A 2019 Improving mechanical properties of continuous fiber-reinforced thermoplastic composites produced by FDM 3D printer *J. Reinf. Plast. Compos.* **38** 99–116